



HAL
open science

A unique combination of in-situ and multi-scale methodologies to analyze damage mechanisms of temper rolled zinc coating

Jean Legendre, Romain Créac'Hcadec, A. Tanguy, S. Hallais, Jean-Hubert Schmitt, E. Hériprié, F. Gilbert, D. Jacquet, J. Mataigne

► To cite this version:

Jean Legendre, Romain Créac'Hcadec, A. Tanguy, S. Hallais, Jean-Hubert Schmitt, et al.. A unique combination of in-situ and multi-scale methodologies to analyze damage mechanisms of temper rolled zinc coating. *Materials Science and Engineering: A*, 2019, 763, pp.138156. 10.1016/j.msea.2019.138156 . hal-02269799

HAL Id: hal-02269799

<https://centralesupelec.hal.science/hal-02269799>

Submitted on 25 Oct 2021

HAL is a multi-disciplinary open access archive for the deposit and dissemination of scientific research documents, whether they are published or not. The documents may come from teaching and research institutions in France or abroad, or from public or private research centers.

L'archive ouverte pluridisciplinaire **HAL**, est destinée au dépôt et à la diffusion de documents scientifiques de niveau recherche, publiés ou non, émanant des établissements d'enseignement et de recherche français ou étrangers, des laboratoires publics ou privés.



Distributed under a Creative Commons Attribution - NonCommercial 4.0 International License

A unique combination of *in-situ* and multi-scale methodologies to analyze damage mechanisms of temper rolled zinc coating

J. Legendre^{1,4}, R. Créac'hcadec¹, A. Tanguy², S. Hallais², JH. Schmitt^{3(*)}, E. Héripéré³,
F. Gilbert⁴, D. Jacquet⁴, J.M. Mataigne⁴

¹ IRDL, CNRS FRE 3744, UBS/ENSTA Bretagne/UBO/ENIB, ENSTA Bretagne, 2 rue F. Verny, 29806 Brest Cedex, France.

² LMS, Ecole Polytechnique, CNRS, Université Paris-Saclay, Route de Saclay, 91128 Palaiseau, France.

³ MSSMat, CNRS, CentraleSupélec, Université Paris-Saclay, 3 rue Joliot Curie, 91190 Gif-sur-Yvette, France.

⁴ ArcelorMittal Global R&D Montataire, BP 30109, 1 route de Saint Leu, 60761 Montataire, France.

Abstract – Coated sheets for car body are assembled by spot-welding and, more and more, by adhesive bonding. Thus, during life time, the coating endures stresses which can lead to the failure of the whole bonded assembly. The behavior of the zinc coating has then to be primarily studied during tension of flat samples. Several investigation techniques, including *in-situ* characterizations and 3D observations, are combined to observe and understand the damage mechanisms of the zinc coating during plastic deformation. A specific attention is paid to the influence of temper rolling which is usually applied on low-carbon steel sheets after annealing and hot-dip coating. Damage is mainly observed at the boundary of large zinc grains lying on the surface plateaus, non-deformed by rolling, and often nucleates at the defects due to dendritic zinc solidification.

Key-words – Zinc coated steel; temper rolling; damage; *in-situ* tensile test; DIC; FIB-SEM

1. Introduction

Low carbon steel sheets for automotive applications are coated with zinc alloy to be protected against corrosion. The great majority of cold-rolled steel sheets for automotive are hot dip coated in a Zn bath at 460 °C after annealing. The coated sheet is then temper rolled to achieve a flat surface, control the roughness and adjust the mechanical properties.

Deep drawn parts are assembled to form the car body. In the body shop, the main assembly technique is spot welding. In addition, the use of continuous adhesive joint is in constant increase as it improves the stiffness and the crash performance of vehicle parts. In fact, the joint strength is critical during crash where all the parts of the bond (adhesive, steel and galvanized layer) can be plastically deformed. This is particularly true in the case of a ductile steel substrate. Automotive equipment manufacturers evaluate the adhesive bonding properties using two criteria: the maximal shear stress value (lap shear test), and the failure pattern. It is worthy to note that an adhesive failure is considered as unacceptable by

(*) Corresponding author: jean-hubert.schmitt@centralesupelec.fr

carmakers. It was recently showed a possible link between the plasticization of the coated steel beneath the adhesive and the failure pattern [1].

Early work already studied the zinc coating behavior accounting for the hexagonal crystallography of grains and crystallographic texture inherited from solidification [2]. A series of papers detailed the damage mechanisms occurring in the zinc layer during straining of coated steel samples [3-6]. However, some controversies still exist to prove whether cracks initiate along the zinc grain boundaries, then lead to decohesion at the steel–zinc interface, or the reverse. Bending and *in-situ* SEM bending experiments were recently proposed to study the behavior of galvanized steel [7,8]. Such experiments are not easy to analyze since bending induces heterogeneous strains within the coating. A second difficulty arises from the observation surface which is the sheet thickness and may be not representative of the damage mechanisms within the whole sample. Moreover, none of these studies accounts for an effect of temper rolling on the zinc coating deformation, except a work studying how the production of zinc fines during a friction test depends on the roughness of the roll surface [9].

The objective of this paper is to explore the deformation and damage mechanisms of a temper-rolled coated steel sheet during straining and give first insights to future work on the fracture mechanisms at the zinc – adhesive interface. Investigation tools at different scales and *in-situ* scanning electron microscopy (SEM) tensile tests coupled with digital image correlations (DIC) are combined to study the coating evolutions during straining of a temper rolled zinc-coated steel sheet. After deformation, FIB-SEM cross-section observations allow an in-depth investigation of the coating and the zinc – steel interface. A special focus is done on the effect of temper rolling, damage propagation during straining, and 3D observation of cracks formation.

2. Experimental procedures

The material under study was a galvanized low carbon ductile steel grade, cold rolled to 0.8 mm, then continuously annealed and hot dip coated. The steel substrate, containing 0.08 wt.% carbon and 0.5 wt.% manganese, has an average grain size about 16 μm .

The thickness of the zinc layer is around 10 μm . A small amount of aluminum (0.2 wt.%) is added to the zinc bath to produce a reactive adhesion of the coating on the steel substrate. A thin layer of intermetallic Al_5Fe_2 is formed between steel and zinc [10,11]. Solidification of zinc on sheet surface gave rise to large grains, of the order between 50 and 200 μm , with a

crystallographic texture which is primarily basal after solidification as already well established [2,11].

At the end of the annealing process, coated sheets were temper rolled, which deformed the zinc layer and locally modified the crystallographic texture and the grain microstructure [11-13].

Dog-bone, full-thickness tensile specimens were cut in the galvanized sheet along the transverse direction. The gage length and width are 8 and 4 mm respectively. The samples were strained with a home-made tensile machine of 5 kN capability, specially designed for *in-situ* tests either under optical microscope (OM) or in a SEM. The displacement rate was chosen to get an initial strain rate of about 7.10^{-4} s^{-1} . Local displacement was measured by DIC. For tests under OM, the surface contrast was increased by air-spraying a speckle pattern of black paint particles on a white painted background. Black dot diameters were between 25 and 100 μm . Two reference points, initially defined, allowed the average elongation to be followed as if it were a “numerical” extensometer. The software Sylvia [14] computed on line the mean strain during the tensile test. From an estimation of the actual section of the sample, a stress-strain curve can then be drawn (Figure 1.a).

As the zinc layer deformation was relatively heterogeneous due to the large grain size, DIC was used to quantify the displacement field and evaluate a representative elementary surface. Images with a resolution of 3296 x 1633 pixels were acquired with an optical camera (Prosilica GX3300 – Allied Vision) at a frequency of a frame per second. Maps of the strain field were calculated with the digital image correlation software CMV [15]. Strain heterogeneities were seen during tensile test. They appeared relatively early during deformation, then tend to slightly decrease at largest applied strains (Figure 1.b to d). The representative elementary surface was then deduced as described by [16] and evaluated to be about $1.8 \times 1.8 \text{ mm}^2$.

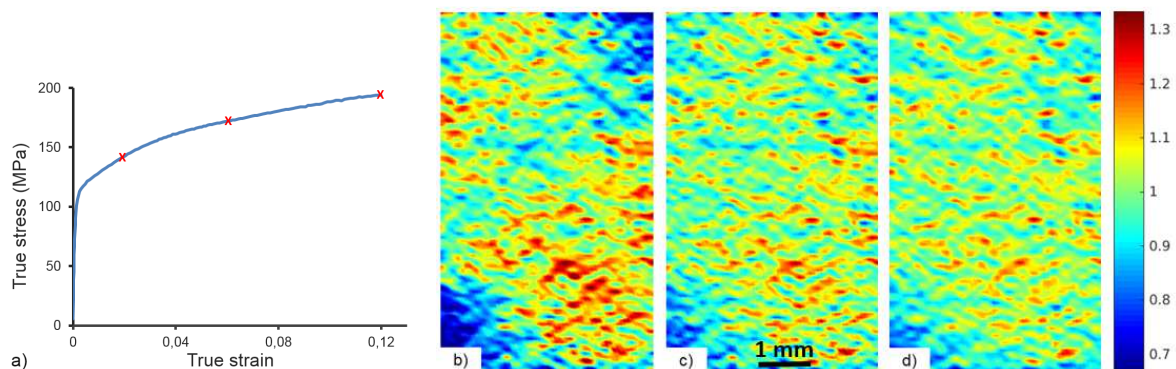


Figure 1 – (a) Tensile stress-strain curve of coated low carbon steel; (b, c, d) Longitudinal strain field of the process zone after 0.02, 0.06, and 0.12 of average macroscopic elongation (the tensile axis is vertical).
The color levels represent the ratio of the local relative strain by the average one.

In order to investigate the local deformation of the zinc layer in more detail, *in-situ* tensile tests were performed in a Field Emission Gun – Scanning Electron Microscope (FEG SEM – FEI QUANTA 600). A thin gold square grid was deposited by electron lithography [17,18]. The mesh was made with regular squares of 2 μm side length. To get a correct image without any shift, the tensile test was stopped at different strains up to 0.12 to allow image capture of the area of interest. During this stage, the tensile force was slightly decreased to avoid any creep. High resolution Back Scattered Electron (BSE) images were taken at 20kV. The CMV software [15,17] was used to compute the strain field from the displacement of the nodes of the square grid. The local deformation could then be correlated to the texture evolution and damage mechanism of the zinc coating.

The crystallographic orientation of zinc and steel grains was deduced from Electron Back Scattering Diffraction (EBSD). The sample surface was first cleaned, then ion polished in order to take off aluminum oxides and carbon traces from the surface while keeping the roughness unchanged. The PECS II System (model 685) by Gatan was used for 5 min polishing at 4 kV with two argon ion beams at an angle of 10° from the surface. The ion polishing highly improves the quality of the EBSD diagrams and strongly reduces the fraction of non-indexed points. EBSD measurements were performed under 20 kV with a spot size of 4 and a step size of 2.5 μm (resp. 0.7 μm) for $3 \times 3 \text{ mm}^2$ areas (resp. $250 \times 250 \mu\text{m}^2$). Grain boundaries were defined for a 10° misorientation between two adjacent domains. The local misorientation gradient, up to 10° , was measured with the Kernel Average Misorientation (KAM), deduced from EBSD maps.

Finally, 3D observations were performed after Focused Ion Beam (FIB) machining through the zinc layer. A gallium ion beam was accelerated under 30 kV in a SEM (FEI Helios Nanolab 660). The beam current was first set to 21 nA to create a regular cross-section, then reduced to 9.3 nA, and finally to 2.5 nA, to clean up the new surface.

3. Results and discussion

3.1. Effect of temper rolling

Temper rolling, sometimes called ‘*skin pass*’, is applied on steel sheets after galvanization to improve their flatness and adjust the final mechanical properties (suppression of the Lüders plateau for low carbon steel, control of the yield strength) [19]. A complementary use of temper rolling is the transfer of a controlled roughness on the sheet using special rolls with a designed surface [11,19,20]. This is of prime importance for the final aspect of painted parts of the car body, and also favors lubrication during deep drawing and stamping of parts [9,20]. Due to a low thickness reduction and an applied tension on the strip, temper rolling mostly affects the sheet surface. For galvanized steel sheets, it means that the zinc layer is primarily deformed [9]. The rolling cylinder roughness is such that some areas are indented which creates valleys on the sheet surface around non-deformed plateaus (Figure 2.a). Between valleys and plateaus, a transient region is mostly subjected to shear stress. The coating surface then appears roughly like the negative of the roll roughness after temper rolling. Band Contrast, which quantifies the quality of the diffraction signal in an EBSD map, clearly highlights plateaus (Figure 2.b). Their average diameter is of the order of 100 to 150 μm . These observations are quantitatively coherent with the sheet roughness measurements after rolling [20].

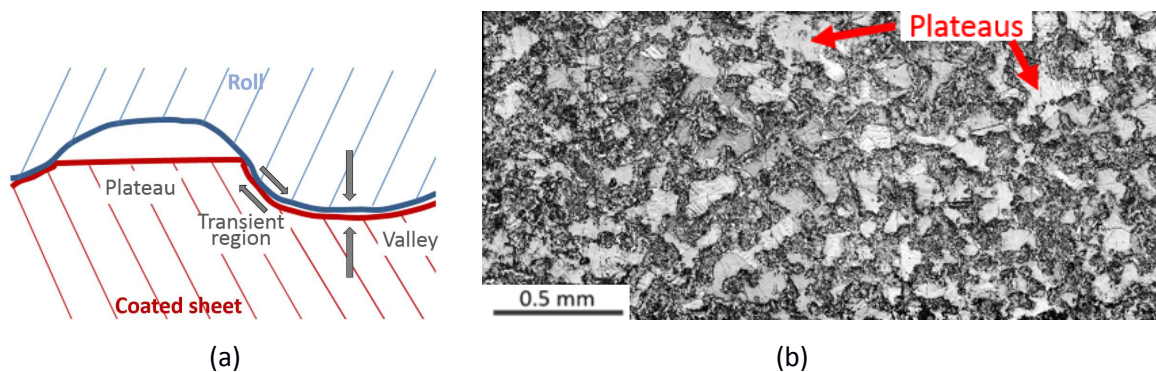


Figure 2 – (a) A schematic description of roughness transfer from roll to sheet surface: valleys are mostly submitted to plane compression, and transient regions to shear;
 (b) EBSD Band Contrast map of the coating surface after temper rolling: the non-deformed plateaus appear as smooth light grey areas.

The sub-surface microstructure is evidenced by KAM measurements which image the grain or sub-grain plastic deformation (Figure 3). Plateaus are in fact large domains with a constant crystallographic orientation (in blue in Figure 3.b). It is to be noted that, in these non-strained areas of the zinc surface, solidification dendrites are often still visible (noted by black arrows in Figure 3.a). A low depression on the zinc surface locates the end of the solidification. This is frequently observed on coating surface before any cold rolling [2]. These traces confirm that

the plateaus had no contact with the roll cylinder during temper rolling. The highest misoriented areas delineate strained regions (noted A and C in Figure 3.b). From EBSD Band Contrast or KAM measurements, the surface fraction of plateau is estimated roughly equal to 50%.

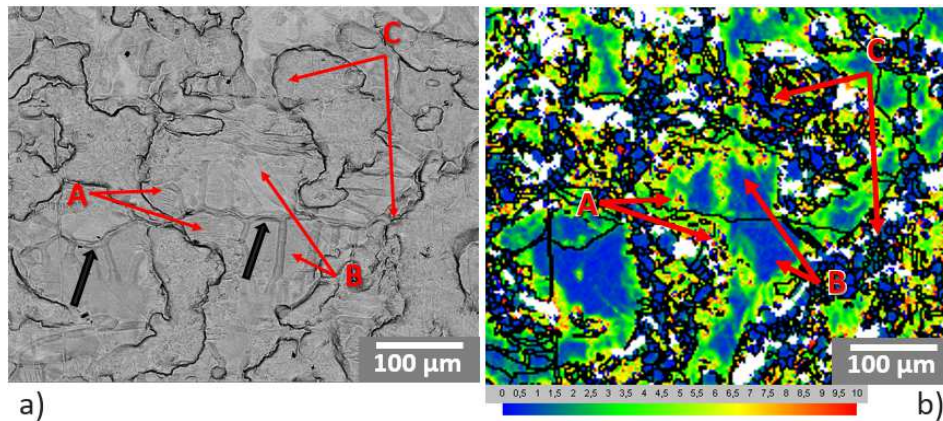


Figure 3 – Zinc surface after temper rolling: (a) BSE image (traces of solidification dendrites are indicated by black arrows); (b) KAM map of the same area (colors quantify the local misorientation from 0 to 10° according to the bar below the figure, and black lines delineate grain boundaries). A, B, and C denote examples of transient regions, plateaus, and valleys respectively, as sketched in Figure 2.a.

EBSD maps also evidence these different domains in connection with the grain size (Figure 4). Though the large scale of the map (3x3 mm²) and the surface roughness complicate an accurate measurement of the crystallographic orientation, almost 70% of the pixels can be indexed. Figures 4.a and b clearly show a bimodal distribution of the grain size in agreement with the local KAM map in Figure 3.b. A careful comparison between Band Contrast and EBSD maps on a same area and the analysis between BSE images and corresponding EBSD maps at higher magnification (Figure 5) allow us to confirm the largest grain size is associated to the plateaus, while the smallest is to the valleys and the transient regions. As an example, the large grain in Figure 5.a, with the $[\bar{1}2\bar{1}0]$ axis at 4° from the z direction on the IPF-z orientation map, was not strained during temper rolling as confirmed by traces of solidification dendrites (black arrow in Figure 5.a). It is then possible to extract from EBSD maps, all grains with a size larger than 40 μm which can reasonably be assumed as lying on the plateaus (Figure 4.c). Their average size is about 90 μm, similar to the grain size after solidification. Most often, these grains extend through the full thickness of the zinc layer (see for instance on the right side of Figure 6). Most of these grains have a basal orientation as observed after solidification and before any temper rolling.

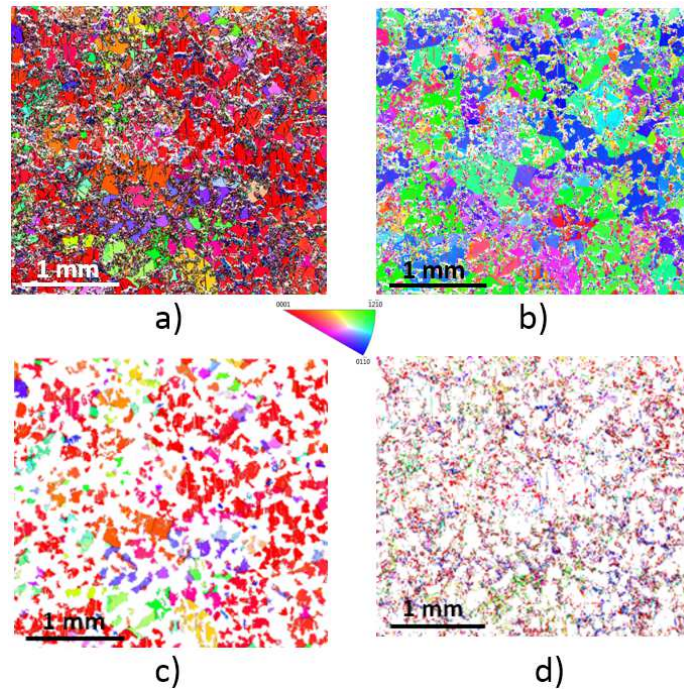


Figure 4 – EBSD maps of the zinc coating surface after temper rolling: (a) IPF coloring for the z-axis normal to the sheet; (b) IPF coloring for the x-axis parallel to the rolling direction (horizontal axis); (c) Orientations of the largest grains (above 40 μm) – IPF-z; (d) Orientation of the smallest grains (below 40 μm) – IPF-z.

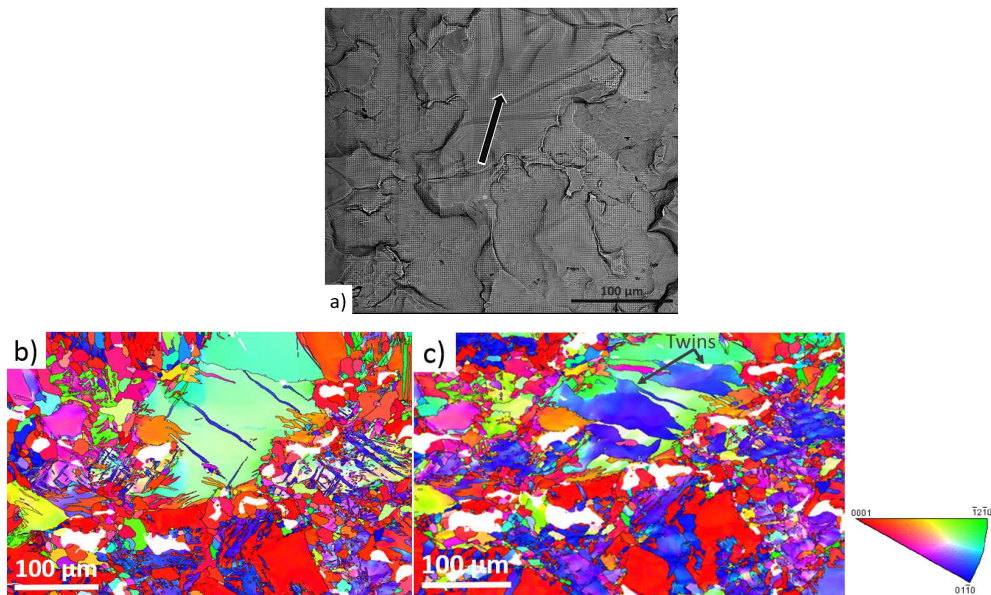


Figure 5 – Effect of temper rolling on the zinc coating (a) BSE observation (the black arrow indicates a dendrite mark on a large grain); (b) EBSD map of the same region (IPF-z); (c) EBSD map after 0.12 strain in tension (IPF-z) (deformation twins are clearly visible in the large grain).

In the valleys, the average grain size is smaller (about 15 μm) and grain orientations are more diverse (Figure 4.d). The size of the valleys is of the order of a few tenths of micrometers,

which is in good agreement with the estimation of the strained surface under a roll indentation calculated by FE simulations [9]. Due to local straining, grains in the valleys and transient regions are subdivided through the coating thickness (Figure 6).

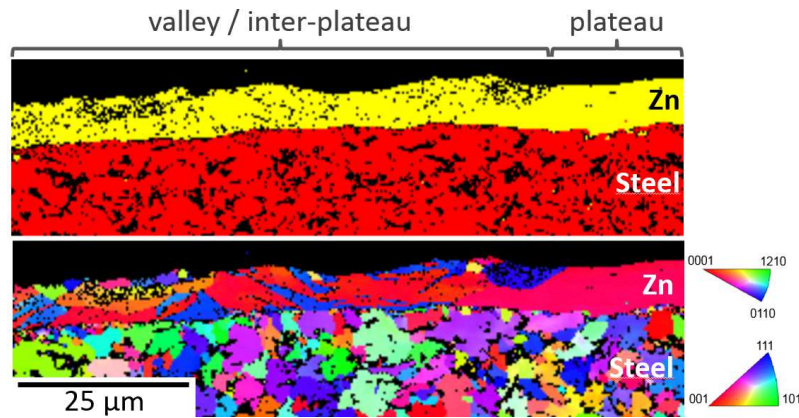


Figure 6 – Through-thickness orientation of Zn grains after temper rolling. IPF-z, z being the normal to the sheet surface.

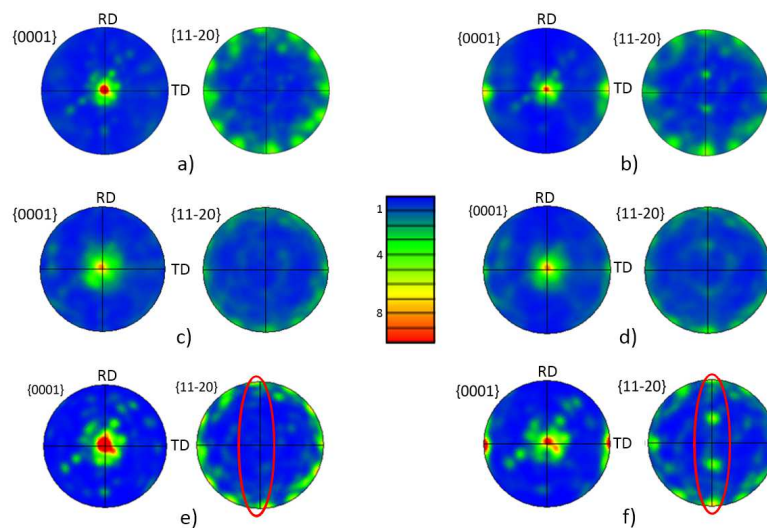


Figure 7 – $\{0001\}$ and $\{11-20\}$ pole figures of zinc grains calculated from $3 \times 3 \text{ mm}^2$ EBSD maps after temper rolling along RD (a, c, and e) and after 0.12 tensile strain along TD (b, d, and f).

(a) and (b) from all grains

(c) and (d) from small grains (below $40 \mu\text{m}$)

(e) and (f) from large grains

It is to be noted that large grains mainly contributed for the texture evolution during tension.

Pole figures are deduced from EBSD maps with all grain sizes, but also for smaller and larger grain sizes (Figure 7). It is worth to note that there is no qualitative difference between the crystallographic orientations for the smallest and largest grain sizes (Figure 7). After temper rolling, the main component is almost a fiber texture around the basal orientation as already observed by Mataigne et al. [11].

3.2. Surface observation of damage propagation during straining

In-situ SEM straining was performed to investigate the deformation and damage mechanisms on the zinc surface. Due to the main crystallographic orientations after solidification and temper rolling, twinning appears as the main deformation mechanism (Figures 7.a and b). Though the orientation of the large grain in figure 5 is not representative of the average texture of the largest grains, twinning is clearly evidenced with almost half of the surface showing twin orientation after stretching (Figure 5.c). While twinning is also seen in smaller grains with basal orientation, the main contribution to the twinning component in the final texture comes from the large grain deformation (Figure 7.f), that is the non-deformed grain by temper rolling.

Figure 8 presents the field of the Von Mises equivalent strain within an area of $300 \times 300 \mu\text{m}^2$, slightly smaller than the representative elementary surface defined formerly, for two average tensile strains of 0.02 and 0.11. Local strain concentrations are clearly evidenced which define a pattern of inclined directions, roughly at $\pm 45^\circ$ from the tensile axis (Figure 8.b). Locally, the maximum local strain can be twice larger than the average macroscopic strain. It is worthy to be noted that the strain heterogeneities appear at very low strains and develop at a same location on the surface as this was observed at the whole sample scale (Figure 1.a). This result is similar to observations on other hexagonal metals as magnesium alloys, for instance [21].

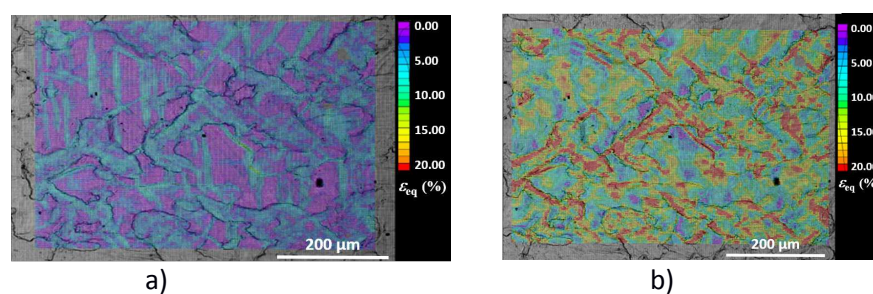


Figure 8 – Local equivalent strain of zinc coating on a $300 \times 300 \mu\text{m}^2$ area for an average strain equal to 2% (a) and 11% (b).

Note the orientation of the strain localization bands, inclined with respect to the tensile axis (horizontal direction)

Mainly due to the limited number of possible slip systems in zinc at room temperature, grain boundary sliding is observed which supplement the intragranular deformation to accommodate the macroscopic strain (Figure 9.b). A quantification of the displacement field

after a strain of 0.12 highlights a deformation only localized at the grain boundary, with almost no intragranular deformation.

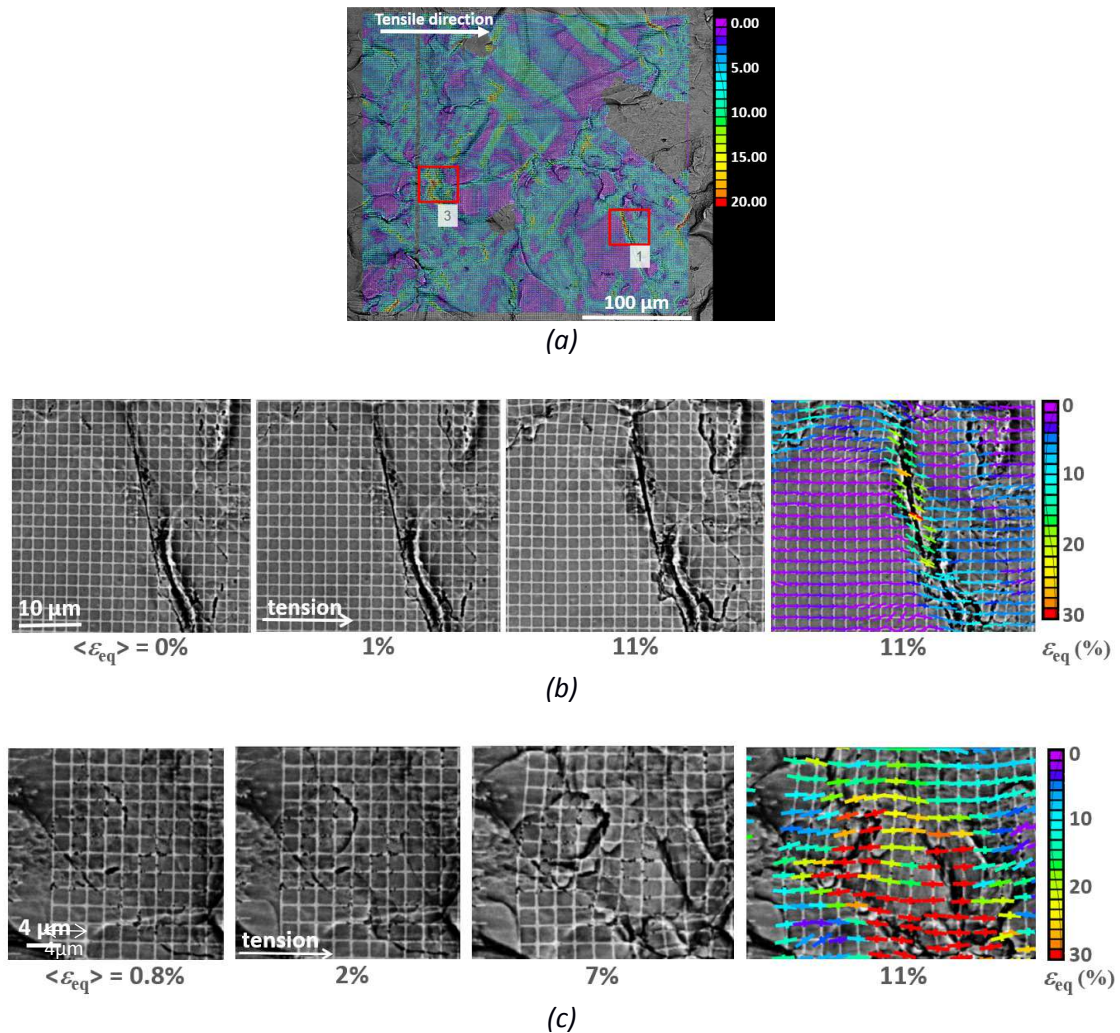


Figure 9 – Surface damage evolution during in situ straining.

(a) Local equivalent strain of zinc coating on a $300 \times 300 \mu\text{m}^2$ area for an average strain equal to 3.7%

(b) Example of grain boundary sliding at different average strains

(enlargement of square 1 in Fig. 9.a).

(c) Example of intergranular crack evolving during straining (enlargement of square 3 in Fig. 9.a)

The last map in (b) and (c) gives the equivalent strain field,
the arrows indicating the direction of the main principal axis of the local strain tensor.

A few cracks are already present after temper rolling, but the majority of them nucleates after a small deformation and opens during straining (Figure 9.c). Cracks often develop along the zinc grain boundaries leading to decohesion between neighboring grains. Triple points are preferred locations for crack initiation, but some can be observed between two grains.

These observations are in good agreement with former results by Parisot et al. [3] and Song et al. [4]. They confirm that cracks might originate from strain incompatibilities between grains with different crystallographic orientations.

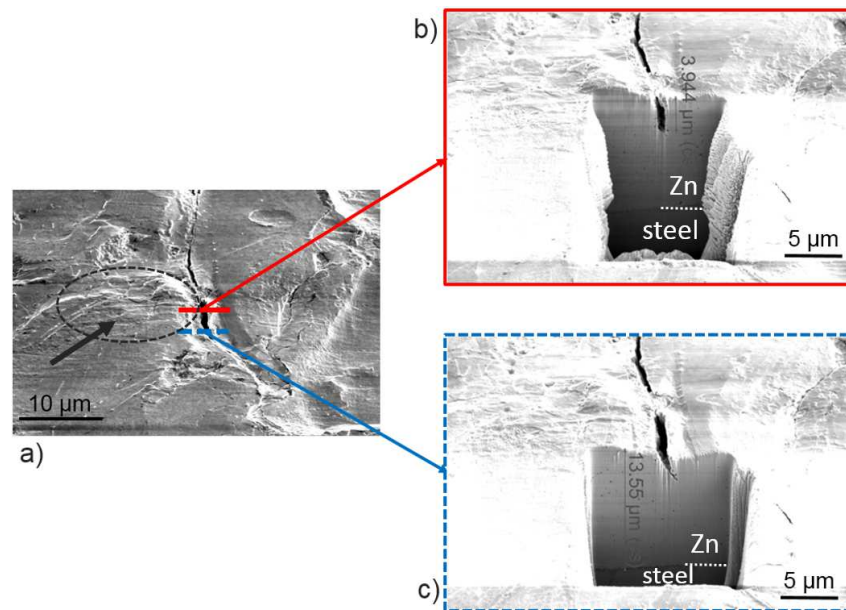


Figure 10 – Crack between two zinc grains in a valley (scratches indicated by an arrow in figure 10.a results from an interaction between the roll and the zinc surface).
a) BSE surface observation after 0.12 strain; b) and c) in-depth view of the cracks at two different locations along the grain boundary after FIB machining.

3.3. 3D characterization of damage within the zinc coating

To go further and investigate the damage mechanism, 3D observations were performed using FIB machining of the zinc surface after straining. Different locations were selected from the *in-situ* tests:

- *On the strained valleys*: Figure 10 shows a crack formed in a valley. Scratches on the surface due to wearing (area indicated by the dotted circle and black arrow in Figure 10.a) confirm that the observation is performed on a strained area. The crack lies along the interface between two zinc grains. As seen during *in situ* experiments, these decohesion cracks slightly propagate along the grain boundary. Their depth seems relatively limited through the zinc layer (Figures 10.b and c). It was never reported any propagation of a crack till the zinc–steel interface. The crack propagation through the coating thickness is most probably limited by twins and grain boundaries (Figure 6), even if the geometry of the hole drilled by FIB does not allow any EBSD measurement to validate this hypothesis. This is coherent with former observations that cracks

initiate on the zinc coating surface [3, 4, 5]. In the valleys, affected by the temper rolling, cracks seem unable to propagate down to the zinc–steel interface.

- *On the non-deformed plateaus:* Cracks frequently nucleate at triple points between grains on the surface (Figure 11). This is where strain accommodation is the most difficult in hexagonal polycrystals [22]. While the crack propagates along the grain boundaries, it also evolves toward the zinc–steel interface (Figure 11). The present observation does not allow us to conclude on the crack initiation location within the coating thickness.

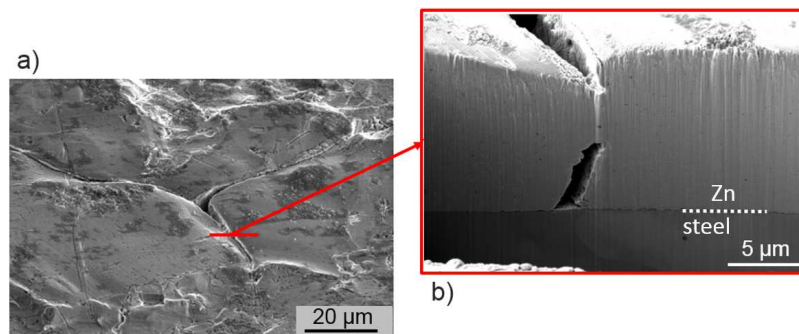


Figure 11 – Crack at a triple point junction on a plateau.
a) BSE surface observation after 0.12 strain; b) in-depth view of the crack after FIB machining.

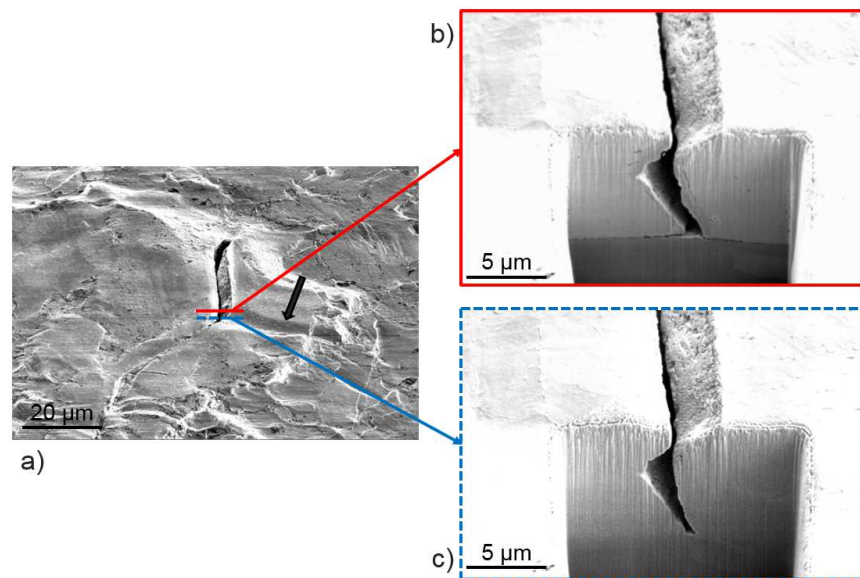


Figure 12 – Crack between two zinc grains on a plateau (note the presence of a trace of dendrite noted by the arrow in Figure a).
a) BSE surface observation after 0.12 strain; b) and c) in-depth view of the cracks at two different locations along the grain boundary after FIB machining.

Cracks are sometimes observed along zinc grain boundaries. In this case, they are always associated with a solidification dendrite. As exemplified in Figure 12, crack initiates at the intersection of a grain boundary and a dendrite (indicated by the black

arrow in Figure 12.a). Crack then clearly propagates along the zinc grain boundary and through the coating thickness until the interface with the steel substrate (Figure 12.b and c). In the central part of the crack, the two zinc grains separate from each other (Figure 12.a). The crack then propagates along the interface between zinc grains and steel substrate (Figure 13). The role of the solidification dendrite in the nucleation process is not totally elucidated. Due to the solidification process, most of the interdendrite grooves delineate a zinc grain boundary (see Figure 3, for instance). Different hypotheses can be stated. First, the intersection between a grain boundary and a dendrite groove is in fact a triple junction, no crack being associated to the dendrite groove due to its orientation with respect to the tensile axis (Figure 12.a). But the nucleation site could also result from a mechanical effect due to the slight groove at the coating surface or an effect of segregated elements in the last solidified liquid which weaken the grain boundary.

An advantage of FIB machining is to allow EDX analyses on the cross section normal to the crack (Figure 13). In this example, a crack propagation is also observed at the interface between the zinc and the Al_5Fe_2 layers. Though the steel grain orientation is not known, the decohesion probably depends on the relative orientation of the zinc and steel grains.

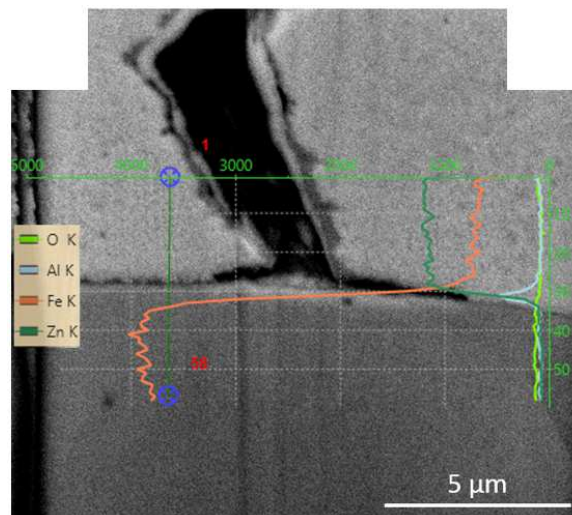


Figure 13 – EDX analysis of the zinc – steel interface after deformation (same cross section as Fig. 12.b).

These 3D observations confirm that the straining of a galvanized low carbon steel sheet induces cracks which nucleate on the surface along zinc grain boundaries, mainly at triple point junctions. Where the zinc coating was locally deformed by temper rolling, the in-depth

propagation of cracks appears limited by the strained microstructure of the zinc layer – twins, sub-grain or grain boundaries. In this case, crack hardly reaches the zinc–steel interface. Conversely, the fact that, in non-deformed areas of the zinc coating (the plateaus), the whole layer thickness containing almost a single grain, cracks which nucleate on the surface propagate through the coating thickness. The main nucleation sites, in these cases, seem to be restricted to the triple points or linked to a solidification dendrite associated to a zinc grain boundary.

4. Conclusions

The present work showed the advantage of coupling different methods at various scales to investigate locally the damage mechanisms of zinc coating. This methodology has been applied for the first time to temper rolled galvanized low carbon steel.

The main results confirm that many cracks nucleate on the zinc surface due to difficulties of strain accommodation between grains of a hexagonal polycrystal, associated to the effect of a free surface. It was proved that, beyond triple points, solidification dendrites can promote nucleation of cracks at zinc grain boundaries.

Temper rolling does not decrease the tendency for crack nucleation and propagation in strained areas (the valleys), but the deformed microstructure through the coating thickness tends to limit, or even suppress, crack propagation until the zinc–steel interface which could be favorable for corrosion resistance and reduction of powdering.

A stronger coupling between *in-situ* observations and 3D characterization opens a real path for a better understanding of the damage mechanisms of zinc coating on steel and its interaction with adhesive.

Acknowledgments – This work was carried out within the MATMECA consortium and supported by the ANR under contract number ANR-10-EQPX-37. The FEG SEM FEI Quanta 600 has been acquired with the financial support of Region Ile-de-France (SESAME 2004 program), CNRS, and Ecole Polytechnique.

References

- [1] J. Legendre – Compréhension et caractérisation multi-échelle de la rupture interfaciale d'assemblages collés (colle crash - tôle galvanisée) pour l'automobile [Multi-scale characterization of interface fracture of glued assembly for automotive applications], PhD dissertation, Université de Bretagne occidentale (Brest, France) 2017. *In French*.

<https://tel.archives-ouvertes.fr/tel-01711967>

- [2] R. Parisot, S. Forest, A. Pineau, F. Grillon, X. Demonet, and J.M. Maigne – Deformation and damage mechanisms of zinc coatings on hot-dip galvanized steel sheets: Part I. Deformation modes, *Metall. Mater. Trans. A* 35A (2004) 797-811.
<https://doi.org/10.1007/s11661-004-0007-x>
- [3] R. Parisot, S. Forest, A. Pineau, F. Nguyen, X. Demonet, and J.M. Maigne – Deformation and damage mechanisms of zinc coatings on hot-dip galvanized steel sheets: Part II. Damage modes, *Metall. Mater. Trans. A* 35A (2004) 813-823.
<https://doi.org/10.1007/s11661-004-0008-9>
- [4] G.M. Song, W.G. Sloof, Y.T. Pei, and J.Th.M. De Hosson – Interface fracture behavior of zinc coatings on steel: Experiments and finite element calculations, *Surface & Coatings Technol.* 201 (2006) 4311-4316.
<https://doi.org/10.1016/j.surfcoat.2006.08.046>
- [5] G.M. Song, and W.G. Sloof – Characterization of the failure behavior of zinc coating on dual phase steel under tensile deformation, *Mater. Sci. Eng. A* 528 (2011) 6432-6437.
<https://doi.org/10.1016/j.msea.2011.04.058>
- [6] G.M. Song, T. Vystavel, N. van der Pers, J.Th.M. De Hosson, and W.G. Sloof – Relation between microstructure and adhesion of hot dip galvanized zinc coatings on dual phase steel, *Acta Mater.* 60 (2012) 2973-2981.
<https://doi.org/10.1016/j.actamat.2012.02.003>
- [7] V. Di Cocco, F. Iacoviello, L. D’Agostino, and S. Natali – Damage micromechanisms in a hot dip galvanized steel, *Proc. 24th Italian Group of Fracture (IGF) Conf., Urbino (Italy), March 1-3, 2017*, F. Iacoviello, L. Susmel, D. Firrao, and G. Ferro Eds., *Procedia Structural Integrity* 3 (2017) 231-236.
<https://doi.org/10.1016/j.prostr.2017.04.054>
- [8] J. He, J. Lian, A. Aretz, N. Vajragupta, U. Hangen, F. Goodwin, and S. Münstermann – Fracture properties of zinc coating layers in a galvanized steel and an electrolytically galvanized steel, *Mater. Sci. Eng. A* 732 (2018) 320-325.
<https://doi.org/10.1016/j.msea.2018.05.084>
- [9] M. Dubar, S. Huart, R. Deltombe, A. Dubois, and L. Dubar – Cold rolling of galvanized strips: A new approach to the evaluation of zinc fines formation, *J. Mater. Process. Technol.* 177 (2006) 505-508.
<https://doi.org/10.1016/j.jmatprotec.2006.03.196>
- [10] L. Chen, R. Fourmentin, and J.R. Mc Dermid – Morphology and kinetics of interfacial layer formation during continuous hot-dip galvanizing and galvannealing, *Metall. Mater. Trans. A* 39A (2008) 2128-2142.
<https://doi.org/10.1007/s11661-008-9552-z>
- [11] J.M. Maigne, V. Vaché, and M. Repoux – Surface chemistry and reactivity of skin-passed hot dip galvanized coating, *Rev. Métall.* 106 (2009) 41-47.
<https://doi.org/10.1051/metal/2009013>
- [12] G. Vincent, F. Zhang, J.J. Fundenberger, and C. Eslin – Experimental and simulation textures in an asymmetrically skin-passed zinc galvanized sheet, *Scripta Mater.* 53 (2005) 775-779.

<https://doi.org/10.1016/j.scriptmat.2005.04.054>

- [13] L. Cauvin, B. Raghavan, S. Bouvier, X. Wang, and F. Meraghni – Multi-scale investigation of highly anisotropic zinc alloys using crystal plasticity and inverse analysis, *Mater. Sci. Eng. A* 729 (2018) 106-118.
<https://doi.org/10.1016/j.msea.2018.05.038>
- [14] D.S. Yang, M. Bornert, S. Chanchole, H. Gharbi, P. Valli, and B. Ghatmiri – Dependence of elastic properties of argillaceous rocks on moisture content investigated with optical full-field strain measurement techniques, *Int. J. Rock Mech. Min. Sci.* 53 (2012) 45-55.
<https://doi.org/10.1016/j.ijrmms.2012.04.004>
- [15] M. Bourcier, M. Bornert, A. Dimanov, E. Héripré, and J. Raphanel – Multiscale experimental investigation of crystal plasticity and grain boundary sliding in synthetic halite using digital image correlation, *J. Geophys. Res. Solid Earth* 118 (2013) 511-526.
<https://doi.org/10.1002/jgrb.50065>
- [16] C. Efstathiou, H. Sehitoglu, and J. Lambrosb – Multiscale strain measurements of plastically deforming polycrystalline titanium: Role of deformation heterogeneities, *Int. J. Plasticity* 26 (2010) 93-106.
<https://doi.org/10.1016/j.jiplas.2009.04.006>
- [17] L. Allais, M. Bornert, T. Bretheau, and D. Caldemaison – Experimental characterization of the local strain field in a heterogeneous elastoplastic material, *Acta Metall. Mater.* 42 (1994) 3865-3880.
[https://doi.org/10.1016/0956-7151\(94\)90452-9](https://doi.org/10.1016/0956-7151(94)90452-9)
- [18] E. Héripré, M. Dexet, J. Crépin, L. Gélébart, A. Roos, M. Bornert, and D. Caldemaison – Coupling between experimental measurements and polycrystal finite element calculations for micromechanical study of metallic materials, *Int. J. Plasticity*, 23 (2007) 1512-1539.
<https://doi.org/10.1016/j.jiplas.2007.01.009>
- [19] M.L. Busch-Milosevic, H. Biausser, A. Fouratier, B. Fournel, M. Grumbach – Évolution récente du skin-pass des tôles minces [Recent developments in the temper rolling of thin sheets], *Rev. Métall. – CIT* 95 (1998) 939-953. (*in French*)
<https://doi.org/10.1051/metal/199895070939>
- [20] O. Pawelski, W. Rasp, W. Zwick, H.J. Nettelbeck, and K. Steinhoff – The influence of different work-roll texturing systems on the development of surface structures on the temper rolling process of steel sheet used in the automotive industry, *Proc. 5th Int. Conf. Metal Forming (Metal Forming 94)*, Birmingham (England) Sept. 13-15, 1994, *J. Mater. Proc. Technol.* 45 (1994) 215-222.
- [21] G. Martin, C.W. Sinclair, and R.A. Lebensohn - Microscale plastic strain heterogeneity in slip dominated deformation of magnesium alloy containing rare earth, *Mater. Sci. Eng. A* 603 (2014) 37-51.
<https://doi.org/10.1016/j.msea.2014.01.102>
- [22] G. Martin, C.W. Sinclair, and J.H. Schmitt – Plastic strain heterogeneities in an Mg-1Zn-0.5Nd alloy, *Scripta Mater.* 68 (2013) 695-698.
<https://doi.org/10.1016/j.scriptamat.2013.01.017>